Progress In Electromagnetics Research C, Vol. 116, 235–248, 2021

Design and Analysis a Frequency Reconfigurable Octagonal Ring-Shaped Quad-Port Dual-Band Antenna Based on a Varactor Diode

Qasim H. Kareem[1, 2, *], Malik J. Farhan[1], and Ali K. Jassim[1]

Abstract—Due to recent developments in wireless communications, frequency reconfigurable antennas have increased in popularity. This paper presents an integrated design for multi-input-multi-output (MIMO) antennas that use octagonal ring-shaped with a frequency-tunable dual-band reconfigurable for wireless communication applications. On the ground plane, the designed antenna has four octagonal ring-shaped radiators with a total size $50 \times 50 \times 1.6\,\text{mm}^3$. In the center of each radiator, a varactor diode is employed to control the capacitive reactance of the slot to provide frequency reconfigurability. Between orthogonally positioned antennas, rectangular defective ground gaps are used for isolation purposes as well. Dual-band operation is achieved by linking the varactor to a slot line of radiating rings. The antenna's lower-frequency band resonates at 4.2 GHz, and its upper-frequency band can be tuned from 4.55 to 5.56 GHz (with isolation > 25 dB in the operating bands). The simulated results are found to be highly consistent with the experimental data. As a result, frequency agility, large tuning range, compactness, and planar structure make it appropriate for a wide range of existing and future wireless communication applications.

1. INTRODUCTION

Modern wireless communication needs processing a high volume of data quickly and efficiently and optimal spectrum utilization to connect an enormous number of devices and permit the flow of a vast amount of data much more rapidly. Wireless portable devices that operate across several frequency standards are regularly enhanced with new features and services. The increased use of many services may result in congestion of the frequency band. Congestion increases the cost of spectrum licensing, resulting in a greater cost per bit for each user. Using frequency reconfigurable MIMO antennas systems in cognitive radio (CR) platforms, it is possible to meet high data rate needs while operating with different wireless standards and efficiently utilizing spectrum resources [1]. To transition between multiple bands and provide smooth and interference-free radiated, frequency reconfigurable antennas are used at the front ends of cognitive radio. Its radio frequency (RF) front end consists of an ultra-wideband (UWB) antenna and a frequency-reconfigurable antenna. The first is used for spectrum detection and the second for multiple communications [2]. The UWB antenna constantly searches for free frequency bands in the wireless networks, while the frequency reconfigurable antenna changes frequencies to transmit inside the detected frequency bands. Although both antennas are necessary, building a compact communication antenna that switches frequency over a broad bandwidth while remaining versatile is more complicated. CR approaches have been developed to maximize the utilization of spectrum resources [3, 4]. Several other types of antennas (monopole, loop, and Printed-IFA) have

Received 17 September 2021, Accepted 11 November 2021, Scheduled 24 November 2021

* Corresponding author: Qasim Hadi Kareem (qasim.hadi2017@gmail.com).

[1] Electrical Engineering Department, Mustansiriyah University, Baghdad, Iraq. [2] Computer Engineering, Al-Farabi University College, Baghdad, Iraq.

been proposed for frequency reconfigurable systems. However, the reconfigurable antenna with double slots based at ground plane is an interesting option for frequency reconfigurable applications because of their low profile, low cost, and planar structure, light weight, ease of manufacture, and ability to integrate readily with various electronic components.

This research aims to develop antennas capable of being controlled in terms of frequency and radiation pattern. The following is the problem statement addressed in this work: Designing, modelling, and fabricating reconfigurable antennas to analyze and investigate how this could be accomplished using a varactor diode as the integrated tuning component. Multiple frequency reconfigurable antennas operating in the 1.5–4.35 GHz range have been reported [5–11]. Frequency reconfigurability was achieved in these designs by including varactor diodes [5, 9], pin diode [7, 11], or micro-electromechanical systems (MEMS) switches [8]. A u-slot microstrip patch antenna with an element area of $77 \times 57\,\text{mm}^2$ was published in [5]. It has a linear input reactance and a controllable frequency range of 2.6 to 3.35 GHz by modifying the input reactance. [6] and [7] proposed dual-frequency reconfigurable patch-slot antennas capable of switching between 1.7 and 3.5 GHz. Five switches were positioned in the slot, each with a patch element size $29 \times 18.3\,\text{mm}^2$. In [8], a frequency reconfigurable E-shaped patched antenna based on MEMS switches was proposed to address complex antenna problems associated with cognitive radio systems. The antenna was capable of switching patterns, frequency, and polarization with a tuning frequency between 2 and 3.2 GHz and patch antenna size of $44.1 \times 92.5\,\text{mm}^2$. A patch slot antenna dual-band system with a capacitor loading slot was proposed in [9]. It can tune the frequency band between 1.45 and 1.93 GHz with a capacitance range of 0.31–0.74 pF and a DC voltage range of 2–30 V. The patch radiator had a surface area of $38 \times 38\,\text{mm}^2$. [10] demonstrated the use of a dual-band unidirectional stacked antenna with double square patches to produce well-controlled frequency-tunability between 1.68 and 1.9 GHz in the low band and 2.11 to 2.51 GHz in the high band. The patch has a thickness of 3.17 mm and a surface area of $82 \times 82\,\text{mm}^2$. In [11], a pattern and frequency are changed by varying the effective length of the patch antenna with the integration of diodes capable of operating at 2.43 and 3.3 GHz with a patch element of $36 \times 30\,\text{mm}^2$. Most published reports for reconfigurable patch antennas utilize a single patch antenna which is too large and has limited bandwidth.

Wireless technologies that require wide bandwidth for data transmission benefit from using a frequency-reconfigurable MIMO antenna system because they are flexible enough to reconfigure their operating frequency. Numerous designs for frequency-reconfigurable MIMO antennas have been published in the literature [12–15]. [12] presented a dual-port reconfigurable MIMO antenna system with a $90 \times 50\,\text{mm}^2$ substrate area based on a quarter-wave slot line on the ground plane. The antenna covered three M-LTE bands: 2.3–2.4 GHz, 2.5–2.7 GHz, and 3.4–3.6 GHz. To achieve reconfigurability, PIN diodes were utilized and placed on the slot line. [13] focused on designing a two-element printed frequency-reconfigurable MIMO antenna with a frequency range of 2.1–2.4 GHz and a bandwidth of 50 MHz. It can be reconfigured by adjusting the DC bias voltage between 0 and 6 V. The patch was compacted using GND annular slots, and reconfigurability was added through a varactor diode. However, the substrate's overall dimensions were $50 \times 100\,\text{mm}^2$. A dual-port reconfigurable MIMO antenna system with a fully metal rim designed for use with LTE/WWAN smartphones was reported in [14]. Excellent isolation across the whole operating band was obtained with substrate dimensions of $145 \times 72\,\text{mm}^2$. [15] described a dual-band frequency tunable MIMO patch-slot antenna with the total dimensions of $120 \times 60\,\text{mm}^2$. At the ground plane, a hexagonal-shaped DGS was used to reduce the size of the antenna and improve isolation. By adjusting the capacitance of the varactor from 2.5 to 35 pF, the frequency can be tuned between 1.3 and 2.6 GHz.

The literature mentions two-element frequency-reconfigurable MIMO systems. Increased data rate and channel capacity are achieved by increasing antenna elements, improving overall system performance. [16–20] presented MIMO antennas with four radiators. In [16, 17], a four-elements modified monopole based on a planner F shaped frequency-tuning MIMO antenna was tailored to cover a wide range of standard systems from 0.7 to 3 GHz with a substrate area size of $120 \times 65\,\text{mm}^2$. Tuning over broadband was accomplished using a combination of PIN and varactor diode. [18] described the design of a tiny quad-port reconfigurable MIMO slot for IEEE802.11 applications. The structure consistsed of four slots, two of which were reconfigurable by including MEMS switches with an overall antenna size of $46 \times 20\,\text{mm}^2$ for each two-port configuration. [19] presented a four-element MIMO antenna with orthogonal U-slots cut from the same cavity to identify the radiating patches. The antenna

design incorporated four varactor diodes into the radiating structure to tune a single band between 4.67 and 5.84 GHz. [20] integrated a reconfigurable wearable MIMO antenna with two switches-enabled hanging resonators and a partial ground plane with funnel-shaped DGS to cover the frequency ranges of 3.11–5.15 GHz in one switching state and 4.81–7.39 GHz in another switching state. [21] presented a frequency-tunable MIMO patch antenna with a reconfigurable feedline. Two hexagonal-shaped antennas with a varactor diode in the microstrip feedline can be tuned between 1.42 and 2.27 GHz with minimum isolation of 12 dB and total dimensions of $100 \times 50\,\text{mm}^2$. [22] described a four-element annular ring-shaped monopole antenna with an orthogonal arrangement for mid-band 5G and WLAN applications. For narrowband tuning, a varactor diode was employed between the feed line and stepped-impedance resonating stubs (3–4.5 GHz and 4.4–6 GHz), and PIN diodes were used to transition between frequency bands. However, the biasing circuit included additional components, complicating production.

Most previous works have focused on non-continuous frequency tuning, single band operation, the absence of reconfigurable slots at the ground plane, high-profile designs, and poor isolation between radiating parts. This work proposes a compact, continuously tuned, dual-band, and high isolation frequency-tunable MIMO antenna with an octagonal-ring slot defective ground structure (DGS) to address these issues. In each ring's slot, a varactor diode is placed to provide reactive loading. Variable bias voltage across the varactor diode allows tuning across a range of frequencies between 4 and 4.35 GHz and a wide range between 4.55 and 5.56 GHz. The antenna with octagonal slot rings supplied by rectangular microstrip lines has the smallest dimensions and highest isolation of any four-elements frequency-tunable multiple antennas that have been proposed so far, as far as we know. The antenna's lower resonant band is tunable between 4 and 4.35 GHz (greater than 25 dB isolation across the operational range). The upper-frequency band is tunable between 4.55 and 5.56 GHz (with 15 dB isolation in the intended band). The designed antenna is characterized by its planar structure, compact size, and large tuning range across various frequency bands. As a result, it is well suited for usage as the front-end for wireless communication applications.

2. DESIGN OF OCTAGONAL RING-SLOT ANTENNA

The characteristics of the dual-band octagonal slot-based with various design parameters are investigated in this section. The configuration of the proposed radiator-element design is shown in Fig. 1. The antenna design is realized on a substrate with a thickness of 1.6 mm, dielectric constant of 4.3, and tangent loss of 0.025. This antenna contains a recursive octagonal-ring slot etched in the ground plane and a 50 Ω rectangular microstrip feed-line. The the employed slot-ring has a gap of 0.7 mm.

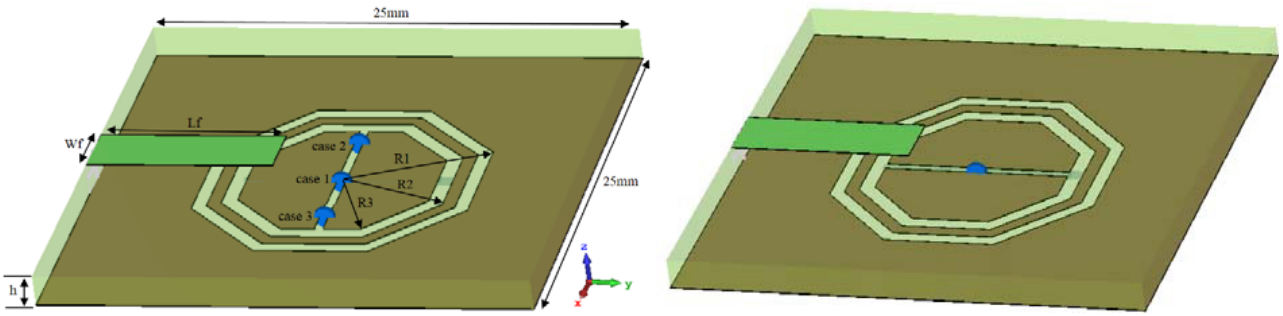

Figure 1. Structure of a radiator element with top and bottom view for: (a) different places of a varactor diode, (b) vertical cut.

The octagonal ring antenna, after careful planning, has multiple-use features, including dual-band and wideband capabilities. According to [23], the equations used to determine the radius (R_1) of the outer octagonal ring are:

$$F = \frac{8.791 \times 10^9}{f_r \sqrt{\varepsilon_r}} \tag{1}$$

$$R_1 = \frac{F}{\left\{1 + \frac{2h}{\pi F \varepsilon_r}\left[\ln\left(\frac{\pi F}{2h}\right) + 1.7726\right]\right\}^{\frac{1}{2}}} \tag{2}$$

where R_1 is the radius of the outer ring, h the substrate's thickness, ε_r the substrate's dielectric constant, and f_r he designed antenna's resonance frequency.

According to Equations (1)–(2), the frequency resonator for the tuning band (4.55–5.56 GHz) is 5 GHz, and other parameters are specifications of the substrate, which include the dielectric constant of the substrate ($\varepsilon_r = 4.3$) and the height of the substrate ($h = 1.6$ mm). All these parameters yield 7 mm for the radius of the outer ring.

Initially, the outer octagonal ring structure has been created with an outer width of 5.8 mm and radius $R_1 = 7$ mm, as shown in Fig. 1(a). Then, based on Equation (1), which uses a recursive process, the width and radius of the ring were kept constant for the simulation and design of the antenna. The recursive concept is based on the fractal qualities of self-repetition and self-similarity. Using this approach, radius $R_2 = 5.6$ mm fits snugly inside the octagonal ring with radius $R_1 = 7$ mm.

To match the impedance, the designed antenna's geometry uses a 50 Ω transmission line. As mentioned previously, the radius of octagonal rings at various iterations is related to the log-periodic approach and may be calculated using the following equation [24].

$$R_{n+1} = \theta \cdot R_n \tag{3}$$

where "n" denotes the number of iterations (1, 2, or 3), and R_1 is the outer octagonal ring's radius. The radius of the designed octagonal ring-shaped is multiplied by the factor (θ), resulting in the radius of the middle ring with radius R_2; this also aids in managing the designed antenna characteristics. The scaling factor θ equal to 0.8 has been tuned to regulate the antenna's design dimensions.

Varactor diodes were unable to use the open slot-based antenna because of the difficulties of reactively loading. However, the center closed slot-line, known to be better able to respond to reactive loading, was also determined to function quite well when utilizing a varactor diode. As a result, the closed octagonal slot-line design was chosen above other open slot-line designs due to its improved radiation properties, good input impedance matching, ease of reactive loading, and optimal area.

The resonant frequencies of the antenna are mainly determined by the radius length of the employed octagonal-ring slots. The first band (4–4.35 GHz) is mainly determined by the radius of the inner octagonal-ring slot. The second resonance (at 5 GHz for the upper band) depends on the value of the capacitance for the outer ring. However, the length of feed-line also has a little effect on the frequency point.

Various configurations of the antenna are shown in Figs. 1(a)–(b). Simulated S-parameter results of the antenna design with different locations (case 1–3) of a varactor diode are shown in Fig. 2(a). As observed, by placing the varactor at the center of the inner ring (case 1), not only the frequency bandwidth of the antenna but also the characteristic of the design have been significantly improved. While in vertical cut (Fig. 1(b)), the characteristics do not change in all cases due to the loading reactance not contributing in their function in contrast to horizontal cut. By changing the radius of the outer ring, the antenna provides good matching with improved bandwidth at a radius (R_1) of 7 mm, as observed in Fig. 2(b). All parameters have been optimized to enable the desired operating frequency band with well-isolated characteristics at the bands. However, the length of feed-line also has a little effect on the frequency point.

Figure 3 shows that the quad-ports octagonal slot-based frequency reconfigurable MIMO antenna system has top and bottom layers denoted by (a) and (b), respectively. The biasing circuitry and microstrip feeding lines are located on the top layer. At the same time, the lower layer is etched with octagonal ring-shaped, and they serve as the common ground plane. The entire area of the substrate is $50 \times 50\,\text{mm}^2$. Furthermore, all radiator elements are arranged symmetrically and orthogonally on the substrate to obtain the same frequency response and diversity characteristics.

3. ANTENNA STRUCTURE

The purpose of this research was to develop a tuning frequency for a four-element dual-band MIMO antenna system that would provide good MIMO performance and isolation between radiators. The

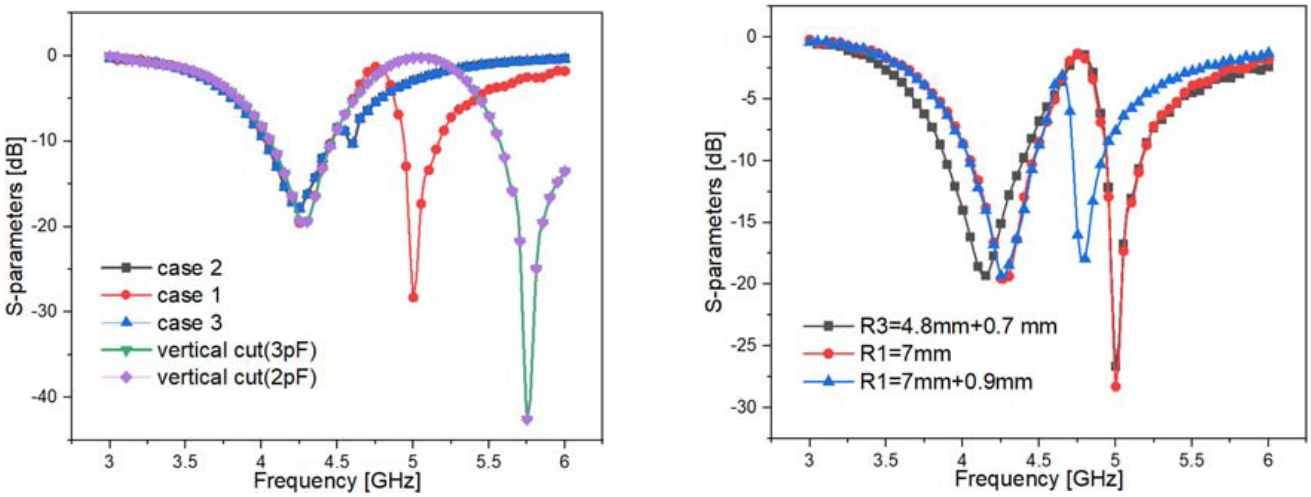

Figure 2. Return lose for (a) vertical cut and cases of the diode places: (b) different values of radius for the inner and outer rings.

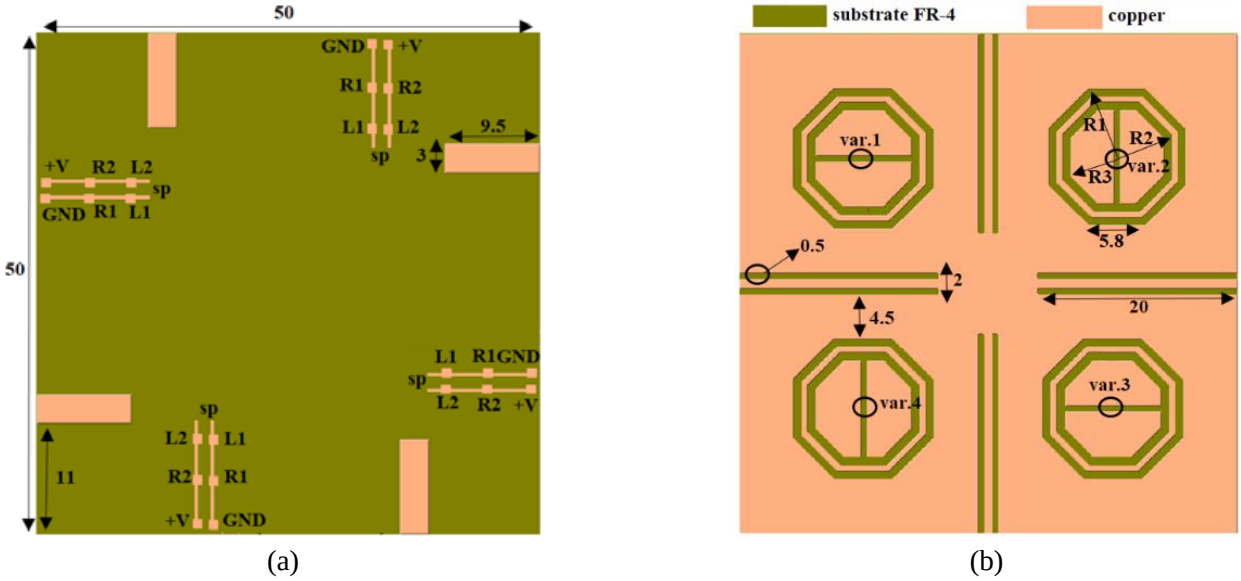

Figure 3. Structure of four-port frequency agile MIMO antenna: (a) top view, (b) bottom view.

proposed work began with a single open slot on a $50 \times 50\,\text{mm}^2$ substrate. Elements can be added to the octagonal closed-loop antenna by using a smaller antenna dimension. Using a 50 ohm microstrip open-ended feed line, each antenna element was stimulated. The designed antenna resonated initially at 4.2 GHz, and excellent agreement between simulated and measured findings is attained, as illustrated in Fig. 4(a). Each antenna was reactively loaded with a varactor diode to optimize it for operation in higher frequency bands. Using parametric sweeps, the optimal location of the varactor diode on the periphery of the center slot was determined, affecting the input impedance matching at higher frequencies. A downsized antenna was made possible by using reactive technology, which reduced the physical size of each antenna element while maintaining performance. Additionally, rectangular line slots in the ground plane that served as DGS further increased isolation between closely spaced radiators.

Figure 4(b) illustrates the simulated reflection coefficient of designed outer and inner ring

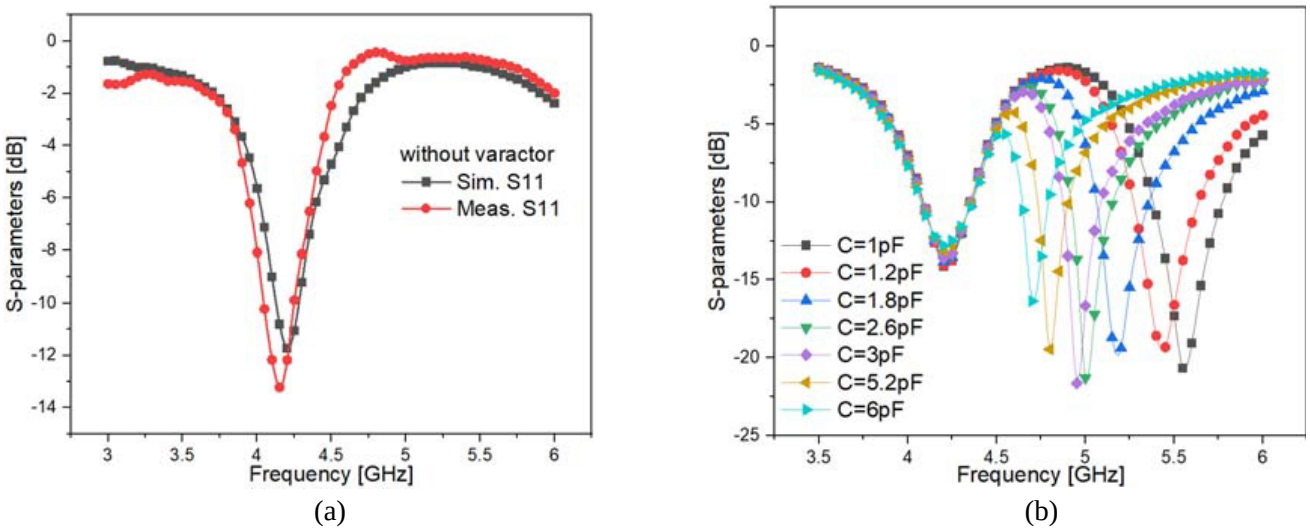

Figure 4. Reflection coefficients simulated and measured: (a) without varactor, (b) with varactor.

structures. It has been demonstrated that by lowering the capacitance value in the structure, the bandwidth improves consistently at each stage and is also enhanced with improved impedance matching. Additionally, the resonance bands between the frequency ranges have been blended as the capacitance value increases, resulting in a wideband response in addition to the multiband response.

DGS's design structure began with placing a rectangular slot between radiators, which resulted in a 0.4 dB increase in isolation. Another rectangular cut contributed to further coupling reduction. However, as indicated in the electric density distribution, many couplings were still seen near the PCB's edges. By introducing DGS slots, the mutual coupling was reduced by at least −0.8 dB.

4. CIRCUIT ANALYSIS OF OCTAGONAL RING-SLOT

According to [25], circuit analysis may be used to estimate the voltages and currents of a device such as an antenna that deals with electric and magnetic fields. For RF antennas, a lumped circuit model can be used to approximate the construction.

As illustrated in Fig. 5(a), the proposed structure comprises three octagonal rings at the bottom of the substrate. Each ring has 2-edges, namely an internal and an external edge. When both rings are analyzed, 4-edges emerge. Due to the substrate beneath the rings and the open space above, it is reasonable to assume that they reside in an inhomogeneous medium. Therefore, the substrate and the open space act as dielectrics, while the ring-edges act as electric plates, resulting in the capacitor's equivalent. Additional edge capacitance is created when similar rings' edges form a single ring's edge. Finally, a capacitance is created by the fact that all 4-edges are coupled together. A total of five capacitances and one resistance exist, which is shown by two octagonal strips with 4-edges each having six combinations.

As shown in Fig. 5(a), a1 and a2 represent the inner and outer edges of the inner octagonal ring-shaped, respectively. In contrast, a3 and a4 represent the internal and external edges of the outer octagonal ring. Thus, each capacitance is labeled to indicate the edges between which it exists. Additionally, Ca12 and Ca34 are capacitances associated with nearby edges, and Ca13, Ca24, and Ca14 are capacitances associated with non-adjacent edges. This results in the exciting finding that capacitances caused by neighboring edges dominate those caused by non-adjacent edges due to the inter-edge distance, which has an inverse effect on the capacitance value.

Additionally, if two points on a single octagonal ring-shaped are considered, it is possible to see a shift in the surface current. Thus, an inductor can be used to realize any two nodes on the surface of each unique ring [26]. Therefore, eight nodes on each edge of the distinct rings are evaluated for analysis, as seen in Fig. 5(a). Fig. 5(c) illustrates an antenna's equivalent circuit in its entirety, including capacitance

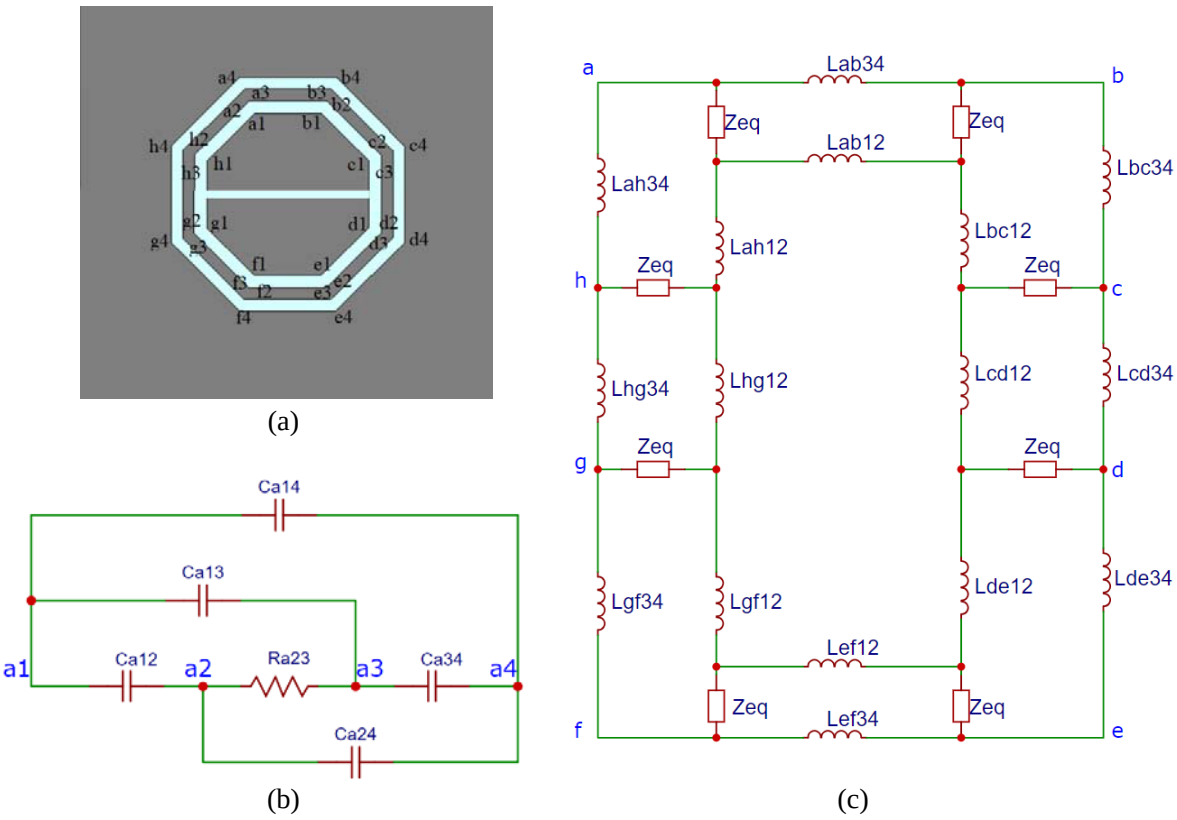

Figure 5. Representation of equivalent circuit: (a) Octagonal antenna with nodes representation. (b) Equivalent capacitive (Ceq) for all edges. (c) Equivalent antenna circuit with inductance and capacitance components.

and inductance components. The inductor is denoted here by the label "Lxymn," where "Lxy" denotes the nodes, and "Lmn" indicates the ring number. Moreover, to simulate all capacitances between edges, each node has been assigned with an equivalent capacitor (Ceq) to account for the total capacitances present, represented by the Ceq (Ceq = Equ (C12, C34, C13, C24, and C14)).

5. BIASING CIRCUIT OF VARACTOR

The biasing network for the proposed frequency-tunable antenna is depicted in Fig. 6. An RF choke inductor (L nH) and a current-limiting resistor (R kΩ) constitute the bias network. The first component (R) protects the varactor diode from the damage caused by forwarding bias and reverses bias leakage

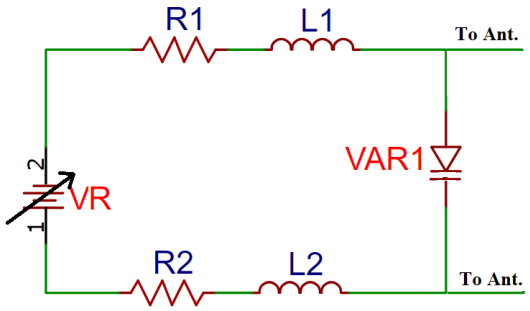

Figure 6. Baising network of varactor diode.

current. The second component (radio frequency choke) separates the antenna radiating structure from the direct current supply. An SMV1763-079LF varactor diode is utilized; the capacitance of this diode can be changed between 1.2 and 9 pF by changing the bias voltage from 0 to 5.5 V [27]. The varactor is represented as a series circuit for full-wave simulations. The parasitic resistance and inductance of the varactor are 0.5 and 0.8 nH, respectively.

Using the CST tool, we execute a full-wave simulation using various capacitance settings to see what happens at capacitance values of 1, 2, 3, 5, and 6. Fig. 4(b) illustrates the reflection coefficients of the designed antenna. Antenna capacitance levels were varied using a reversed bias varactor diode. As a result of the varying capacitance values achieved, distinct resonance frequencies were observed in the system. While retaining robust impedance matching higher than 10 dB, a continuous frequency tuning capability for upper bands from 4.55 to 5.6 GHz can be obtained. In the lower band, the simulated peak gain is 4.76 dBi, whereas in the upper band, it is 2.91 dBi. High-frequency signals and high bias voltages boost the peak gain of the circuit.

6. RESULTS OF PROPOSED DESIGN

CST tool was used to model and optimize the designed frequency-reconfigurable MIMO antennas. The design was optimized by parametric sweeps over many factors, including the slot's width and radius, the location of the varactor diode, and the best spacing between vertically arranged antenna parts. The top and bottom views of the manufactured quad-port frequency reconfigurable MIMO antenna system are shown in Fig. 7. The fabricated model's port parameters were determined using a KC 901V vector network analyzer (VNA).

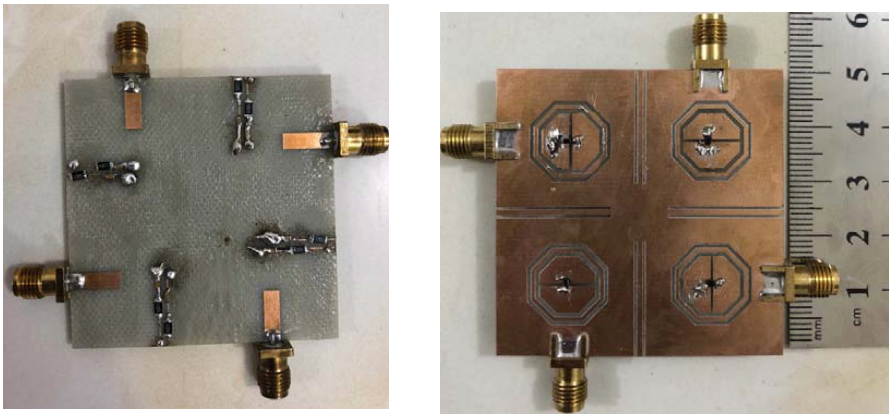

(a) (b)

Figure 7. Fabrication of the designed MIMO antennas: (a) Top view. (b) Bottom view.

6.1. Reflection and Transmission Coefficients

In order to figure out the values of the scattering parameters of the proposed antenna, different voltage levels were tested across the diode. The modeling software used the lumped circuit, which corresponds to the varactor diode. The variable capacitor was made to reflect the information provided in the varactor diode's datasheet. The optimized design for one antenna reflection and transmission coefficients are presented in Figs. 8(a), (b). Due to the identical structure of all antenna elements, identical behavior was found for other antennas.

There is a high degree of agreement between the measured and simulated reflection coefficients curves. Due to the biasing circuit and manufacture tolerances, slight differences in the results values were found. As the DC voltage increases, the frequency increases, and the capacitance across the varactor is lowered. When no voltage was placed between its terminals, 0 V, the varactor had a capacitance of more than 6 pF. The antenna resonates at 4.2 and 4.6 GHz when being connected to 0.2 V. Smooth

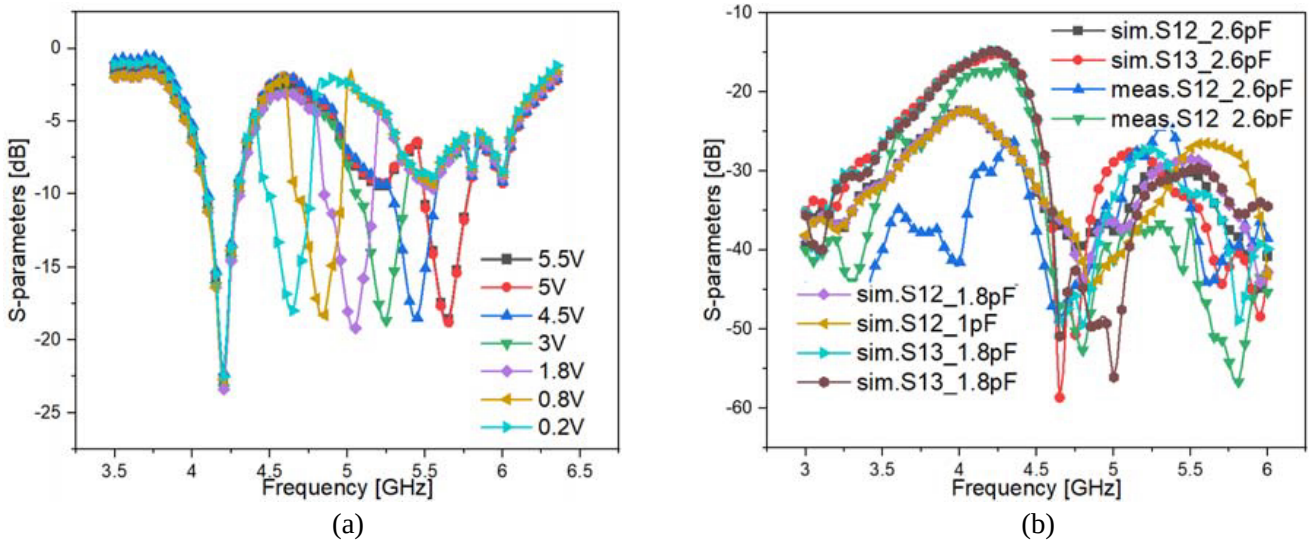

Figure 8. *S*-parameters measured of designed antenna: (a) Measured reflection coeff. (b) Simulated and Measured transmission coeff.

frequency sweeps were detected by raising the reverse bias voltage across the varactor diode, as seen in Fig. 6(a). The varactor had a capacitance of 1 pF, and the antenna resonated at 5.5 GHz when the voltage was 5.5 V. The resonance frequency remained unchanged even though a different reverse voltage was applied to the varactor. Using voltage settings of 0 and 5.5 V, the antenna's bandwidth was configured throughout a 4.55 to 5.56 GHz frequency range, and the antenna had a minimum and maximum 10 dB bandwidths of 147 and 395 MHz.

Isolation is a critical characteristic in the MIMO system, and higher values are preferable for improved MIMO performance since they result in higher efficiencies. The DGS slots enhanced the isolation between adjacent radiators. The proposed design considered the isolation between antenna elements (Ant.1 and Ant.2) and between antenna elements (Ant.1 and Ant.3). Between Ant.1 and Ant.3, the worst-case isolation was observed, and the measured and simulated isolation curves are also displayed in Fig. 8(b). As shown, various cases of biasing voltage were taken into account to observe the isolation between the ports. However, all instances do not affect the lower band, but a slight change is achieved at upper bands due to more energy distributed in the inner ring radiator, which is responsible for higher frequencies. In operating bands, minimum isolation of 15 dB between radiators was observed for varying capacitance values and equal physical distance between elements. This explains why we noticed improved isolation between antennas. The worst-case isolation measured was 15 dB in the lower band (Band-1), whereas other working bands demonstrated lower values.

6.2. Electric Energy Distribution

Figure 9 depicts the antenna's electric energy densities (*E*-fields) with and without DGS at 4.21 and 5 GHz. We see that the outer octagonal ring radiator is more effective (distributes more energy) at lower frequencies (4.21 GHz). However, the inner ring radiator is more effective (distributes more energy) at higher frequencies (5 GHz). The distribution of E-energy density explains the mutual coupling phenomenon. An excited port is used during the simulation of the E-energy distribution process, while all other ports are terminated by 50 Ω. Along the open ring resonator, the E-density distribution is significantly concentrated, demonstrating that this ring positively impacts the antenna's performance at the required working bands. The isolation level in MIMO antennas is determined by how far apart the components are, so their arrangement is crucial to the isolation level. This can be seen in terms of insertion loss and electric energy distributions when decoupling constructions and orthogonal arrangements of the components are incorporated. As a result, at lower frequencies, the mutual coupling is more significant than at higher frequencies. DGS effectively isolated the antennas

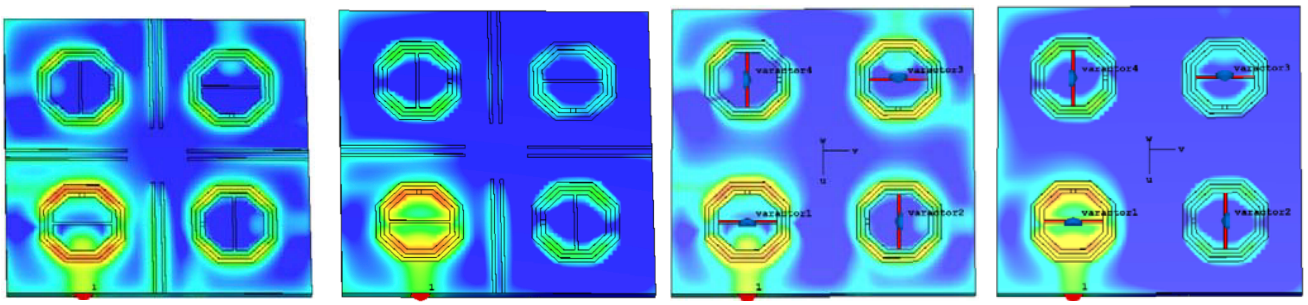

(a) (b) (c) (d)

Figure 9. Electric energy density for Ant.1: (a) lower band with DGS, (b) upper band with DGS, (c) lower band without DGS, (d) upper band with DGS.

from the radiating structure, confirming the isolation enhancement as shown in Figs. 9(a)–(b). So, the DGS slots efficiently reduced mutual coupling between closely placed antenna elements.

6.3. Far Field Radiation Pattern

The antenna elements used in this work have quasi-omnidirectional radiation patterns that mainly cover the top and bottom sides of the PCB. Fig. 10 shows a 3D transparent representation of the radiation patterns for two antenna elements (Ant.1 and Ant.3) operating at 4.21 and 5 GHz.

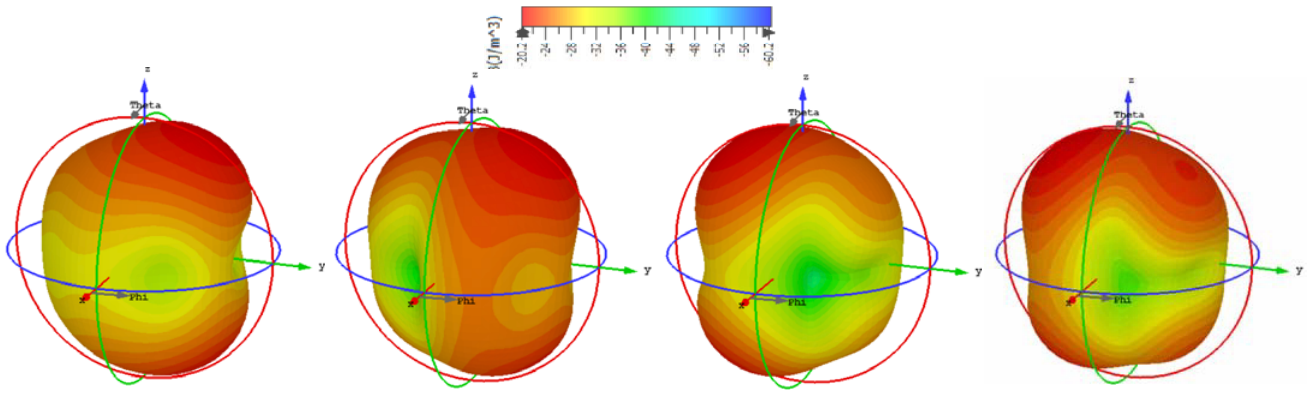

(a) (b) (c) (d)

Figure 10. 3D *E*-field radiation pattern: (a) lower band Ant.1, (b) upper band Ant.1, (c) lower band Ant.3, (d) upper band Ant.3.

As observed that the radiation pattern of the ring-shaped antenna is bidirectional (quasi-omnidirectional), which transmits electromagnetic waves in both the forward and backward directions. Directional antennas are preferred for line-of-sight communication (LOS). However, MIMO antennas are well suited for the use in multi-path non-line-of-sight environments. The MIMO antennas design uses various signal paths to provide data rate improvements in multiple ways. Due to this, an antenna system's directivity is no longer critical for MIMO operations.

Figure 11 shows that the antenna's Co-Pol and X-Pol 2-D electric radiation patterns may be seen in the xy-plane and yz-plane at 4.21 and 5 GHz. Measuring the radiation patterns included using one port and setting up a load of 50 on the remaining ports. Between the proposed MIMO antennas and the transmitter antenna, a 1 m separation was kept. As a result, the measured strength of the signal varied according to how the antenna was moved in the xy- and yz-planes. As a result, the observed data is sufficiently consistent with the simulated data. At a diode capacitance of 2.6 pF, the peak

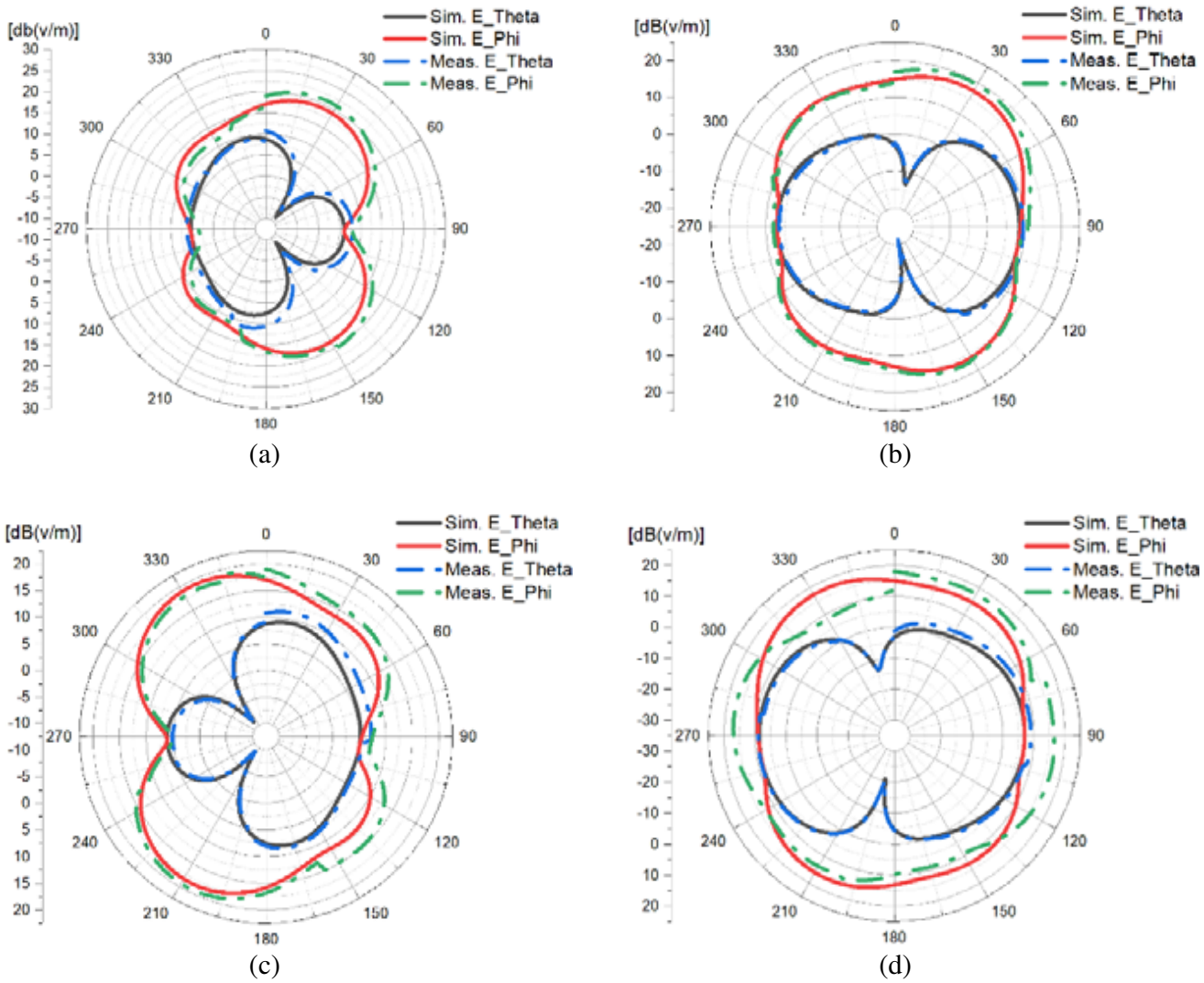

Figure 11. The proposed MIMO antennas system's electric radiation patterns in the xy and yz-plane. (a) Lower band Ant.1. (b) Upper band Ant.1. (c) Lower band Ant.3. (d) Upper band Ant.3.

gain varies between 3.5 and 4.46 dBi in the lower-frequency band (4.21 GHz) and 1.3 to 3.2 dBi in the upper-frequency band (5 GHz). Thus, at 2.6 pF, the efficiency ranges between 63 and 68% for the lower (4.21 GHz) and higher (5 GHz) frequency bands. At 1.8 pF, the efficiency ranges between 45 and 62%, and the peak gain ranges between 2.45 and 2.8 dBi for the higher frequency band (5.18 GHz), respectively. Considering the losses due to impedance mismatch, conduction, and dielectric, the total efficiency will be less than the radiation efficiency by factors of approximately 0.94 and 0.96 for lower and higher bands, respectively.

6.4. Diversity System Performance

The same DC bias can be used to tune the reconfigurable element of the proposed octagonal ring-shaped MIMO antenna, which can be tuned simultaneously. In this situation, the capacity of the channel is significantly increased by optimizing the signals in a multipath environment. The minimum isolation level throughout the lower band is 15 dB, while the maximum isolation level across the upper band is 25 dB. Envelope correlation coefficient (ECC) and diversity gain (DG) are two parameters used to evaluate the MIMO antenna system's performance. The first parameter may be calculated using the

following equation [28]:

$$\mathrm{ECC} = \rho_{eij} = \frac{\left| \iint_{4\pi} \left[F_i(\theta,\phi) \cdot F_j^*(\theta,\phi) \right] d\Omega \right|^2}{\iint_{4\pi} |F_i(\theta,\phi)|^2 \, d\Omega \iint_{4,R} |F_j(\theta,\phi)|^2 \, d\Omega} \tag{4}$$

where $F_i(\theta,\phi)$ represents the radiation pattern associated with ith element, and $\cdot$ indicates the Hermitian product. The maximum calculated ECC across the operational bands when return loss is 10 dB is 0.11. The estimated ECC value generally meets the $\rho_{eij} < 0.5$ criteria for acceptable channel characteristics [28].

The second parameter is analyzed to mitigate fading effects by integrating antenna elements with different fading characteristics. The DG exhibits the improvement in performance produced by the four-elements over a single element. In an ideal situation, the maximum DG is 10 dB. Using Equation (5) provided below [28], the calculated DG is 9.96 dB:

$$\mathrm{DG} = 10\sqrt{\left(1 - |0.99\rho_e|^2\right)} \tag{5}$$

The proposed dual-band octagonal ring quad-port system is compared to previous works. As displayed in Table 1, the designed system has a relatively small size $50 \times 50\,\mathrm{mm}^2$ despite being constituted of four radiating elements. Compared to [15, 18, 19, 21], the proposed design has dual-bands, which has the advantage of smoothly tuning the operational higher frequency band individually or concurrently without impacting each other. Furthermore, the presented compact design exhibits strong isolation and gain due to orthogonal alignment of radiating antennas, which introduces pattern variety and helps in achieving the isolation of more than 15 dB between radiators without the use of complex decoupling components.

Table 1. Comparison with previous works.

Ref.	No. of antennas	Element dimensions (mm^2)	Substrate size (mm^2)	Bands achieved (GHz)	Isolation (dB)	Gain (dBi)	Peak Eff. (%)	ECC
[15]	4	22×14	120×60	1.3–2.6	> 12	1.9–2.48	48, 78	0.2
[16]	4	20×51	120×65	0.78–1.23 1.49–1.76	> 12	-2.1–1.7	N.M.	0.15, 0.18
[17]	4	56.6×17.7	120×65	0.74–1 1.17–2.4	> 12	-0.77–3.52, -2.18–3.44	34, 78	0.021, 0.123
[18]	4	46×20	92×40	2.4–2.5 4.9–5.72	> 14	0–2.9	41, 55, 85	0.2
[19]	4	12×12	30×30	4.67–5.84	> 15	0.4–3.73	65	0.11
[21]	4	29×29	100×50	1.42–2.27	> 12	-0.2–2.2	78	0.2
[22]	4	35.8×16	90×90	3–4.5, 4.4–6	> 13	2.9–3.9	50, 70	0.15, 0.5
Prop. work	4	14×14	50×50	4–4.35, 4.55–5.56	> 15 > 25	1.3–3.2, 3.5–4.46	45, 63, 68	0.01, 0.07

7. CONCLUSION

This work presents a quad-port dual-band reconfigurable MIMO antenna system based on a reconfigurable octagonal ring-shaped antenna. The proposed design provides dual-band characteristics, and reconfigurable frequency tuning is available from 4 to 4.35 GHz for the antenna's lower-frequency

band and 4.55 to 5.56 GHz for the antenna's upper-frequency band. By varying the biasing voltage of the varactor diode, a smooth frequency sweep can be generated. To prevent both direct current shorting and alternate current coupling, the biasing of the varactor diode is implemented using a lumped capacitor. The antenna structure consists of four octagonal rings that are orthogonal to one another and are etched into the ground plane with rectangular-shaped DGS. The presented antenna structure has several advantages: a small overall size ($50 \times 50\,\text{mm}^2$), a planar shape, a low profile, a low cost, no radiation disturbance from biasing lines, and ease of manufacture. In addition, lower band isolation is greater than 15 dB, whereas upper band isolation is greater than 25 dB. Based on the test results, the simulated and measured outcomes demonstrate that the presented antenna is frequency reconfigurable in dual-bands and highly tunable; it is also very stable, making it possible to generate enough radiation patterns and obtain an acceptable ECC value. Due to this, the newly designed antenna can be applied in various applications, such as software-defined radios and cognitive radios, which need frequency reconfigurability.

ACKNOWLEDGMENT

The authors would like to thank Mustansiriyha University (www.uomustansiriyha.edu.iq) Baghdad, Iraq for its support in the present work.

REFERENCES

1. Hussain, R., A. Raza, M. U. Khan, A. Shammim, and M. S. Sharawi, "Miniaturized frequency reconfigurable pentagonal MIMO slot antenna for interweave CR applications," *International Journal of RF and Microwave Computer-Aided Engineering*, Vol. 29, No. 5, 1–12, 2019.
2. Christodoulou, C. G., "Cognitive radio: The new frontier for antenna design?," *IEEE Antennas and Propagation Society*, 2009.
3. Valenta, V., R. Marlek, G. Baudoin, M. Villegas, M. Suarez, and F. Robert, "Survey on spectrum utilization in Europe: Measurements, analyses and observations," *Proceedings of the 5th International ICST Conference on Cognitive Radio Oriented Wireless Networks and Communications*, Vol. 92, 15, 2010.
4. Mitola, J., "Cognitive radio architecture evolution," *Proceedings of the IEEE*, Vol. 97, No. 4, 626–641, 2009.
5. Yang, S.-L. S., A. A. Kishk, and K.-F. Lee, "Frequency reconfigurable U-slot microstrip patch antenna," *IEEE Antennas and Wireless Propagation Letters*, Vol. 7, 127–129, 2008.
6. Majid, H. A., M. K. A. Rahim, M. R. Hamid, N. A. Murad, and M. F. Ismail, "Frequency-reconfigurable microstrip patch-slot antenna," *IEEE Antennas and Wireless Propagation Letters*, Vol. 12, 218–220, 2013.
7. Majid, H. A., M. K. A. Rahim, M. R. Hamid, and M. F. Ismail, "Frequency reconfigurable microstrip patch-slot antenna with directional radiation pattern," *Progress In Electromagnetic Research*, Vol. 144, 319–328, 2014.
8. Rajagopalan, H., J. M. Kovitz, and Y. Rahmat-Samii, "MEMS reconfigurable optimized E-shaped patch antenna design for cognitive radio," *IEEE Transactions on Antennas and Propagation*, Vol. 62, No. 3, 1056–1064, 2014.
9. Khidre, A., F. Yang, and A. Z. Elsherbeni, "A patch antenna with a varactor-loaded slot for reconfigurable dual-band operation," *IEEE Transactions on Antennas and Propagation*, Vol. 63, No. 2, 755–760, 2015.
10. Ge, L., M. Li, J. Wang, and H. Gu, "Unidirectional dual-band stacked patch antenna with independent frequency reconfiguration," *IEEE Antennas and Wireless Propagation Letters*, Vol. 16, 113–116, 2017.
11. Khan, M. S., A. Iftikhar, A.-D. Capobianco, R. M. Shubair, and B. Ijaz, "Pattern and frequency reconfiguration of patch antenna using PIN diodes," *Microwave and Optical Technology Letters*, Vol. 59, No. 9, 2180–2185, 2017.

12. Lim, J., Z. Jin, C. Song, and T. Yun, "Simultaneous frequency and isolation reconfigurable MIMO PIFA using PIN diodes," *IEEE Transactions on Antennas and Propagation*, Vol. 60, No. 12, 5939–5946, 2012.
13. Raza, A., M. U. Khan, R. Hussain, F. A. Tahir, and M. S. Sharawi, "A 2-element reconfigurable MIMO antenna consisting of miniaturized patch elements," *IEEE International Symposium on Antennas and Propagation (APSURSI)*, 655–656, 2016.
14. Xu, Z., Y. Sun, Q. Zhou, Y. Ban, Y. Li, and S. S. Ang, "Reconfigurable MIMO antenna for integrated-metal-rimmed smartphone applications," *IEEE Access*, Vol. 5, 21223–21228, 2017.
15. Zhao, X. and S. Riaz, "A dual-band frequency reconfigurable MIMO patch-slot antenna based on reconfigurable microstrip feedline," *IEEE Access*, Vol. 6, 41450–41457, 2018.
16. Hussain, R., M. S.Sharawi, "Planar four-element frequency agile mimo antenna system with chassis mode reconfigurability," *Microwave and Optical Technology Letters*, Vol. 57, No. 8, 1933–1938, 2015.
17. Hussain, R. and M. S. Sharawi, "Planar meandered-F-shaped 4-element reconfigurable multiple-input-multiple-output antenna system with isolation enhancement for cognitive radio platforms," *IET Microwaves Antennas and Propagation*, Vol. 10, No. 1, 45–52, 2016.
18. Soltani, S., P. Lotfi, and R. D. Murch, "A port and frequency reconfigurable MIMO slot antenna for WLAN applications," *IEEE Transactions on Antennas and Propagation*, Vol. 64, No. 4, 1209–1217, 2016.
19. Boukarkar, A. and X. Q. Lin, "Miniaturized frequency-tunable self quadruplexing four-element MIMO antenna system," *IET Microwaves Antennas and Propagation*, Vol. 14, No. 7, 973–979, 2020.
20. Biswas, A. K. and U. Chakraborty, "Reconfigurable wideband wearable multiple input multiple output antenna with hanging resonator," *Microwave and Optical Technology Letters*, Vol. 62, No. 3, 1352–1359, 2020.
21. Riaz, S., X. Zhao, and S. Geng, "A frequency reconfigurable MIMO antenna with agile feedline for cognitive radio applications," *International Journal of RF and Microwave Computer-Aided Engineering*, Vol.30, No. 3, e22100, 2020.
22. Mathur, R. and S. Dwari, "Frequency and port reconfigurable MIMO antenna for UWB/5G/WLAN band IoT applications," *International Journal of RF and Microwave Computer-Aided Engineering*, Vol. 31, No. 7, 1–11, 2021.
23. Sharma, N. and S.-S. Bhatia, "Metamaterial inspired fidget spinner shaped antenna based on parasitic split ring resonator for multi-standard wireless applications," *Journal of Electromagnetic Waves and Applications*, Vol. 34, No. 10, 1–20, 2020.
24. Mark, R., N. Mishra, K. Mandal, P.-P. Sarkar, and S. Das, "Hexagonal ring fractal antenna with dumb bell shaped defected ground structure for multiband wireless applications," *AEU-International Journal of Electronics and Communications*, Vol. 94, 42–50, 2018.
25. Cheng, D. K., *Fundamentals of Engineering Electromagnetics*, Prentice-Hall Inc., New Jersey, 1993.
26. Hayt, W., J. Kemmerly, and S. Durbin, *Engineering Circuit Analysis*, McGraw-Hill, New York, 2007.
27. SMV1763-079LF: Hyperabrupt Junction Tuning Varactors Datasheet.
28. Kareem, Q. H. and M. J. Farhan, "Design a linear and circular polarization MIMO antennas based on compact size configurations with high isolation and stable gain characteristics for C-band and WLAN/WiMAX applications," *International Journal of Intelligent Engineering and Systems*, Vol. 14, No. 3, 458–467, 2021.